Geostatistical Analysis and Mitigation of Atmosphere Induced Phase in Terrestrial Radar Interferometric Observations of an Alpine Glacier

Simone Baffelli, ETH Zürich, baffelli@ifu.baug.ethz.ch, Switzerland
Othmar Frey, ETH Zürich / Gamma Remote Sensing, frey@ifu.baug.ethz.ch, Switzerland
Irena Hajnsek, ETH Zürich / German Areospace Center (DLR), hajnsek@dlr.de , Germany

Abstract

Terrestrial Radar Interferometry is used to map surface displacement velocites with high temporal resolution, irrespective of sunlight and cloud cover. The main factor limiting estimation accuracy are variations in the atmospheric refractive index, observed as atmospheric phase screens (APS). A statistical model for APS assuming a separable spatio-temporal covariance structure is described. It facilitates the extrapolation of the APS from observations at persistent scatterers (PS) using regression-Kriging, which is followed by a timeseries inversion to estimate the surface velocity. A statistical analysis of the APS is performed using a Ku-Band radar timeseries of Bisgletscher, a glacier in the Southwestern Swiss Alps. The results show that, while some non-stationarity in the covariance structure is observed at large timescales, the covariance models obtained assuming separability perform well in APS mitigation using regression-Kriging.

1 Introduction

Terrestrial radar interferometers (TRI) can be used to estimate the surface velocity of glaciers[1]–[3] using differential interferometry. These observations are complimentary to those obtained from space- and airborne SAR systems: the limited spatial coverage of TRI data is accompanied by an higher flexibility in acquisition time and imaging geometry, permitting to better capture faster temporal dynamics such as diurnal cycles. TRI measurements are also complimentary to non-radar techniques such as time-lapse cameras and total stations because observations are possible regardless of weather and illumination conditions. As TRI is a coherent technique, its sensitivity to changes of the dielectric properties of the propagation medium can severely affect estimation accuracy: the temporal and spatial variability in atmospheric water vapor content[4] cause phase contribution that can, at worst, completely mask the displacement phase. Since these two contributions usually have distinct spatial and temporal statistical behavior[5], it may be possible to estimate their relative contributions and improve displacement estimation accuracy. If a suitable statistical model is used, the uncertainty in the estimates can be quantified as well.

2 Methods and Data

2.1 Signal Model

The problem of estimating displacements from a set of M interferometric phases is formalized as:

$$\mathbf{z} = \frac{4\pi}{\lambda}\mathbf{T}\mathbf{v} + \epsilon_{atm} + \epsilon_{decorr}. \tag{1}$$

Where $\mathbf{z}$ is a stack of M unwrapped and referenced interferograms, comprising of P pixels computed from a vector $\mathbf{s}$ of N SLC (Single Look Complex) acquisitions, ordered by acquisition time. Formally, these two vectors are related by the incidence matrix $\mathbf{A}$ of the interferogram network[6]:

$$\mathbf{z} = \mathbf{A}\mathbf{s}. \tag{2}$$

Furthermore, $\mathbf{v}$ is a vector of $PS, S \leq M$ velocities and $\mathbf{T} = \mathbf{I} \otimes \mathbf{T}_i$ is a block-diagonal diagonal of P blocks. The i-th block, $\mathbf{T}_i$ expresses the relation between the interferometric phase and the velocity for the i-th pixel; usually the same model is used for all pixels. This can be illustrated with an example: assuming a single velocity for the duration of the stack, each block corresponds to the vector of temporal baselines and the problem of (1) reduces to interferogram stacking[7].
The vectors ϵ_{atm} and ϵ_{decorr} represent the (differential) APS and the decorrelation noise affecting the interferometric stack; they are assumed to be mutually

uncorrelated Gaussian random vectors, with a covariance matrix $\mathbf{\Sigma}_z = \mathbf{\Sigma}_{z,atm} + \mathbf{\Sigma}_{z,decorr}$[5].
The optimal estimate of $\mathbf{v}$ in the above model is the generalized least squares (GLS) solution[8]:

$$\hat{\mathbf{v}} = \left(\mathbf{T}^T \mathbf{\Sigma}_z^{-1} \mathbf{T}\right)^{-1} \mathbf{\Sigma}_z^{-1} \mathbf{T}\mathbf{z} \tag{3}$$

However, problems of theoretical and practical nature imply that a direct solution of (3) is often not possible:

- The covariance matrices of the APS and of the decorrelation are not known a priori.
- Even if they were, their inversion would be computationally costly.

2.2 Noise Model and Inversion Scheme

Solving (3) directly may be not necessary if simplified structures for $\mathbf{\Sigma}_z$ and for the displacement model are assumed.
To begin, one should remember that the APS affecting an interferogram between the i-th and the j-th acquisitions is in fact a *differential* APS, the difference between the unobservable APS affecting the SLC phases of the two data takes.
The SLC APS is modeled statistically as a Gaussian random processes (GRP) with well defined mean and covariance functions, $\mu(\mathbf{s}, t)$ and $C_y(\mathbf{s}, \mathbf{s}+\mathbf{d}, t, t+u)$. The mean function $\mu(\mathbf{s}, t)$ is identified with the effects of atmospheric stratification[2], [9]–[12], described through a linear model in the spatial coordinates. The covariance function C is needed to fully describe the random behavior of the atmosphere, which is attributed to turbulent mixing[4].
As interferograms are computed by differencing SLC phases at the same location for different times, they will be again samples of GRP since linear combinations of GRP are again GRP. Since the mean function was assumed to be a linear function of the coordinates, the same functional form can be used to describe the differential stratified APS. However, the covariance function C_z of the differential APS is a function of two pairs of acquisition times and not just two times as in C_y.
Therefore, some simplifying assumptions are needed to estimate the second order statistics of the APS and to use them to improve the estimation of surface displacements described in 3.
Thus, the SLC APS is assumed to be isotropic, stationary in time and space and separable, so that the covariance between any two points and times is only a function of the temporal and spatial separations d and τ and can be factored in a temporal and a spatial covariance function[13]:

$$C_y(\mathbf{s}, \mathbf{s}+\mathbf{d}, t, t+u) = C_{y,s}(d)\, C_{y,t}(\tau) \tag{4}$$

Its discretization at the SLC pixel locations and times give the covariance matrix $\mathbf{\Sigma}_y$; thanks to separability it can written as the Kronecker product of temporal and spatial covariance matrices, $\mathbf{\Sigma}_{y,s}$ and $\mathbf{\Sigma}_{y,t}$:

$$\mathbf{\Sigma}_y = \mathbf{\Sigma}_{y,s} \otimes \mathbf{\Sigma}_{y,t} \tag{5}$$

This translates to the following covariance matrix $\mathbf{\Sigma}_z$ for the differential APS:

$$\mathbf{\Sigma}_z = \mathbf{\Sigma}_{y,s} \otimes \mathbf{A}^T \mathbf{\Sigma}_{y,t} \mathbf{A} \tag{6}$$

This implies that the spatial covariance of the APS affecting interferograms in $\mathbf{z}$[5] is the same as the one of the SLC APS. As stationarity is assumed, the covariance is only a function of distances between pixels and not of their locations. Similarly, the temporal covariance is solely a function of the temporal baseline and of the incidence matrix $\mathbf{A}$. A similar covariance model was proposed in[5]; the main difference being the assumption that the APS is uncorrelated in time, which is realistic in the spaceborne SAR case, where revisit times of several days are common.
Arguably, these are strong assumption on the statistical character of the APS; they are clearly violated by assuming Taylor's hypothesis[14], where turbulent structures are advected by the wind, resulting in a non-separable covariance[13]. However, spatio-temporal stationarity and separability can be employed to simplify the inversion of (3) in the following manner:

- $\mathbf{\Sigma}_{atm,s}$ and $\mathbf{\Sigma}_{atm,t}$ are estimated using a variogram estimator on a set of persistent scatterers (PS) located on stable areas, where $\mathbf{v} = 0$ and where no decorrelation is expected. Specifically, $\mathbf{\Sigma}_{atm,s}$ is estimated by averaging spatial variograms over the set of all avialable interferograms. $\mathbf{\Sigma}_{atm,t}$ is estimated as the average variance of interferometric phases as a function of the temporal baseline.
- the APS at any point for the i-th interferogram is predicted with regression-Kriging[15] using the phase measured at the PS and the estimated spatial covariance. After removing the APS prediction, the interferogram $\mathbf{z}_{res}$ is approximatively spatially uncorrelated.
- Solve (3) replacing $\mathbf{z}$ with $\mathbf{z}_{res}$ and $\mathbf{\Sigma}_{atm,s}$ with $\mathbf{I}$. Since the spatial correlation is removed, the problem can be now solved for each pixel individually by only accounting for temporal correlation.

2.3 Displacement Model and Interferogram Network Formation

The assumption of a displacement model through $\mathbf{T}$ and $\mathbf{v}$ also has bearing on the solution of equation (3). Using a model with $S \ll PM$ increases the robustness of the estimates by providing redundant observations; additionally with a wise choice of displacement model, together with the above assumptions regarding the covariance of the APS, the large inversion problem of (3) can be split into subproblems that can be solved independently.
In this case, a piecewise linear model with a constant velocity v_j over a duration t_s covered by a group of interferograms with length N_s is used. Thus, considering a single pixel, the problem matrix $\mathbf{T}_i$ is:

$$\mathbf{T} = \frac{4\pi}{\lambda} \begin{bmatrix} T_{11} & 0 & \dots & 0 \\ \vdots & \vdots & \dots & \vdots \\ T_{N_s 1} & 0 & \dots & \vdots \\ 0 & T_{12} & \dots & \vdots \\ \vdots & \vdots & \dots & \vdots \\ \vdots & T_{N_s 2} & \dots & 0 \\ \vdots & 0 & \dots & T_{1S} \\ \vdots & \vdots & \dots & \vdots \\ 0 & 0 & \dots & T_{N_s S} \end{bmatrix} \tag{7}$$

where the entry T_{ij} corresponds to the time duration spanned by the i-th interferogram in the j-th stack. For all P pixels in the i-th stack the problem can be written as:

$$\mathbf{z}_i = (\mathbf{T}_i \otimes \mathbf{I})\, \mathbf{v}_i + \epsilon_{z,i} \tag{8}$$

When $S = 1$, this model corresponds to the case of interferogram stacking[7] where a single velocity for all times is assumed.

3 Experimental Data and Results

3.1 Experimental Data

A three month long series of SLC data was acquired in 2015 with the purpose of monitoring the Bisgletscher, a steep alpine glacier in the Southwestern Swiss Alps, canton of Valais. The data was acquired using KAPRI[16], a polarimetric extension of GPRI, a Ku-Band real aperture terrestrial radar interferometer[17]. The acquisition repeat time was set to 2:30 minutes to minimize decorrelation and phase wrapping, since a maximum displacement rate of up to 2 meters/days is expected in the steepest sections of the glacier.
Since the entire time series would be to large to analyze as a whole, a subset is obtained by randomly selecting 10 reference dates and taking all the SLC within an hour from each of these dates. The goal of this sampling procedure is to ensure a diversity of atmospheric conditions to better characterize the statistics of the APS.

3.2 Displacement Model and Interferogram Network Formation

To minimize phase wraps and maintain high coherence, SLCs separated by a maximum of 7 minutes are used to form interferograms; each group of interferograms thus chosen covers approximatively $t_s = 30$ minutes.

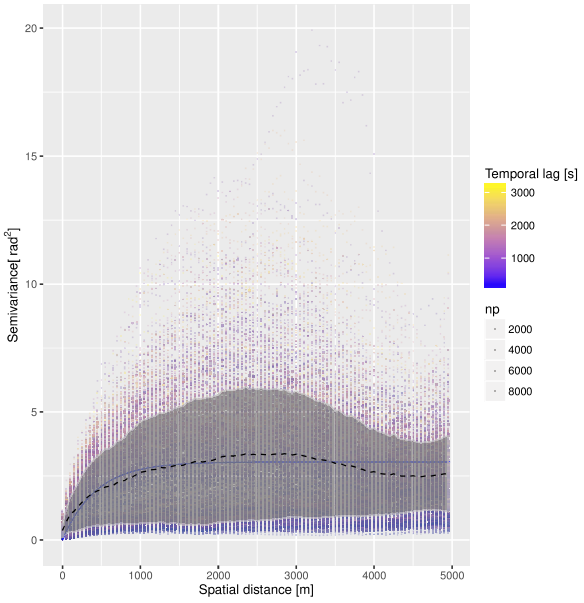

Figure 1: Spatial variogram plot; each dot represents the semivariance at a given spatial lag for a given interferogram, whose temporal baseline in seconds is encoded by the dot's color. The continuous blue line represents an exponential spatial variogram model fit, fitted to the variograms averaged over the set of all temporal lags, shown as the dashed black line. The gray ribbon shows the standard deviation of the variograms.

A set of PS is identified by computing the mean to standard deviation ratio of the intensity of SLC data; the initial set is reduced to approx. homogeneous spatial density[18] using the average interferometric coherence as a quality measure; since the deformation at the timescale of the investigation presented here

is spatially confined to the glacier, it can be safely assumed that their phase is mostly affected by the APS only. These PS are used to compute the spatial and temporal statistics of the APS and to perform regression-Kriging.

3.3 Covariance Model

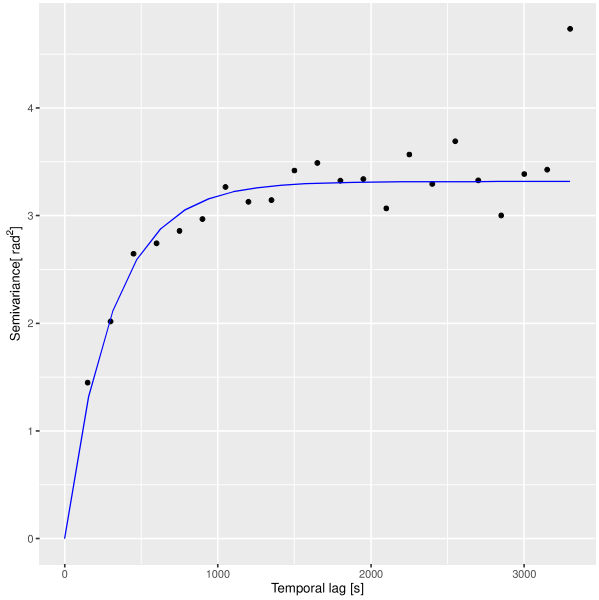

Figure 2: Temporal variogram plot, computed as the mean squared of the interferogram's phases grouped by temporal baseline. The black dots represent the variogram's samples, while the blue line is an exponential temporal variogram model fit.

The validity of assuming a separable spatio-temporal covariance structure is investigated empirically by variogram analysis. All interferograms up to a maximum temporal baseline of one hour are generated from the set of PS; then a spatial variogram is estimated on each interferogram individually; the result of this procedure is shown in Figure 1 as a spatial lag versus semivariance plot. Each dot represents the semivariance at a certain spatial lag for an individual interferogram. The dashed line represents the average variogram obtained by averaging the variograms over the set of all interferograms, while the gray ribbon displays the standard deviation computed over the same set as a function of the spatial lag.
There seems to be a certain variability in variogram's shape as a function of the temporal baseline. Variogram at smaller temporal lags show a longer range, those at longer temporal separations show a shorter range with a larger variation in shape, especially at mid spatial lags. This effect is clearly manifest in the ribbon plot as the different shapes of the lower and upper edges.
Arguably, these results might suggests the inapplicability of a stationary and separable variogram model as described by (5). Namely, if stationarity and separability are assumed, the variogram's shape cannot change with temporal baselines; only its sill –that is the value of the phase dispersion at infinite spatial separation, roughly corresponding to the interferogram's phase variance– can change, scaled by the temporal covariance function; since space-time interactions that would change the variogram's shape are not allowed under a separable covariance model.
Indeed, the value of the sill seems to consistently increase with increasing temporal baselines, as shown in the temporal variogram plot of Figure 2.
Temporal non-stationarity could explain the variation of variogram's shapes: it is likely that different atmospheric conditions are observed at different times of the day, these changes are likely driven by the amount of solar radiation. Evidence for this hypothesis is provided in Figure 3, where the variogram analysis is performed by grouping interferograms by the hour of the day. The results seem to show two main variogram types, reminiscent of those observed in Figure 1 at the upper and lower ranges of the ribbon plot.

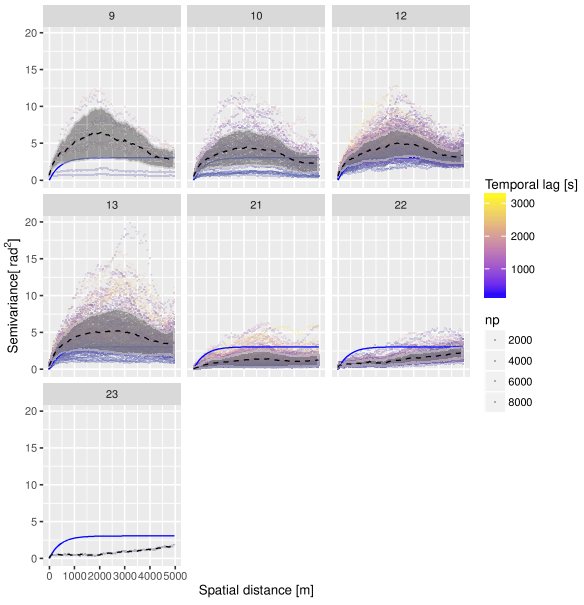

Figure 3: Spatial variogram plot obtained in the same manner as described in Figure 1; variograms are aggregated by the hour of the day and the analysis is repeated for each group individually.

However, the variation in variogram's shape does not seem so severe to warrant the use of a non-separable or nonstationary covariance model, also because of

the higher computational cost of inverting (3) when stationarity and separability are dropped.
The spatial and temporal variogram models estimated assuming stationary separability, while not entirely correct, are used to approximate the spatio-temporal covariance functions of the APS. These covariance models are employed for regression-Kriging and in the GLS inversion for the velocity timeseries.

3.4 Performance of Spatial APS Mitigation

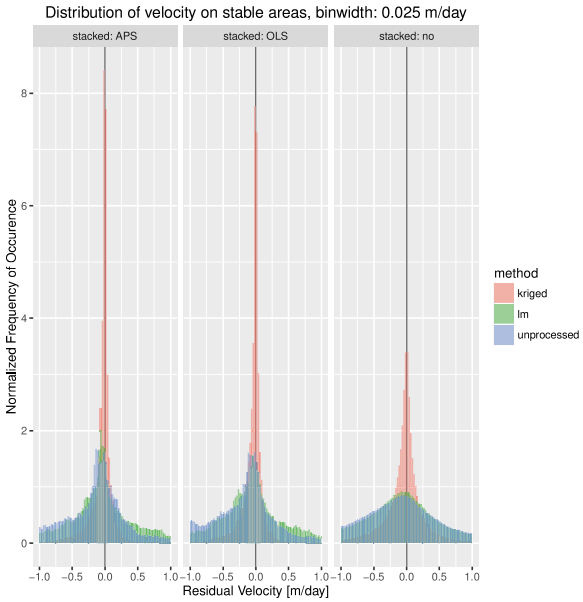

Figure 4: Performance assessment of regression-Kriging in combination with different temporal covariance models for the inversion of (3). The three columns represent the case considering the temporal covariance of the APS (*stacked: APS*), the ordinary least squared result assuming temporally uncorrelated APS (*stacked: OLS*) and the velocities estimated directly from individual interferograms (*stacked: no*).

The performance of regression-Kriging in the mitigation of APS contribution is tested by cross-validation with a set of pixels corresponding to stable areas, taken from all the interferograms in the network. Their phases are extracted, converted into velocities and analyzed by plotting their distribution. The results are displayed in Figure 4 in the column named "*stacked: no*", where the histogram's colors encode the method of APS correction. If no correction is applied ("*unprocessed*"), a skewed and wide distribution is observed. By removing the estimated stratified contribution ("*lm*") the distribution is centered but a significant variance in the estimates is still observed; which is substantially reduced by regression-Kriging ("*kriged*"); probably the stratified APS model is only able to capture a fraction of the total APS phase variance. The relatively high performance of Kriging suggests that the spatial covariance model derived by assuming separability, although not entirely correct and theoretically not justifiable, could be sufficient to mitigate most of the spatial variability caused by the APS.

3.5 Timeseries Inversion Performance

The performance of the timeseries inversion using the derived temporal covariance model, is tested in the same manner as done for the spatial APS mitigation. The results are plotted in the columns of figure 4 named "*stacked: OLS*" and "*stacked: APS*". In the first case, the temporal correlation of the APS is ignored and $\Sigma_{z,t}$ is assumed to be the identity matrix; giving the ordinary least squares (OLS) estimate of $\mathbf{v}$. In the second case, the temporal covariance model estimated by variogram analysis is used to invert (3). Both cases are repeated for different spatial APS mitigation methods; encoded by different colors. The variance is significantly reduced for all spatial APS correction methods in both the OLS and the GLS solution; the latter case with a slightly smaller variance. This plots also highlights another advantage of first applying a spatial APS mitigation: a given level of estimation variance can be achieved by including less interferograms in (7) compared to just solving (8) using interferograms without any APS correction; better preserving the temporal resolution of the estimated velocities.

4 Conclusions

In this paper, a separable spatio-temporal covariance model to describe the APS in high repat-rate terrestrial radar interferometric observations in alpine valleys is presented and tested with geostatistical methods. While variogram analysis shows a partly non-stationary behavior of spatial APS statistics, approximate spatial and temporal statistics are derived assuming separability and used to mitigate the APS using regression-Kriging followed by a generalized least squares inversion for the surface velocity. The choice appears reasonable considering the significant reduction in estimation variance, assessed in a cross-validation analysis on a set of stable scatterers.

References

[1] R. Caduff, F. Schlunegger, A. Kos, and A. Wiesmann, "A review of terrestrial radar interferometry for measuring surface change in the geosciences," *Earth Surface Processes and Landforms*, vol. 40, no. 2, pp. 208–228, 2015.

[2] N. Dematteis, G. Luzi, D. Giordan, F. Zucca, and P. Allasia, "Monitoring alpine glacier surface deformations with gb-sar," *Remote Sensing Letters*, vol. 8, no. 10, pp. 947–956, 2017.

[3] D. Mecatti, L. Noferini, G. Macaluso, M. Pieraccini, G. Luzi, C. Atzeni, and A. Tamburini, "Remote sensing of glacier by ground-based radar interferometry," *International Geoscience and Remote Sensing Symposium (IGARSS)*, pp. 4501–4504, 2007.

[4] R. F. Hanssen, *Radar Interferometry*, ser. Remote Sensing and Digital Image Processing 2. Dordrecht: Springer Netherlands, 2001, vol. 2, pp. 46–53.

[5] P. S. Agram and M Simons, "A noise model for insar time series," *Journal of Geophysical Research : Solid Earth*, no. May 2014, pp. 1–20, 2015.

[6] R. Lanari, F. Casu, M. Manzo, G. Zeni, P. Berardino, M. Manunta, and A. Pepe, "An overview of the small baseline subset algorithm: a dinsar technique for surface deformation analysis," in *Pure and Applied Geophysics*, 4, vol. 164, Basel: Birkhäuser Basel, 2007, pp. 637–661.

[7] T. R. Emardson, M Simons, and F. H. Webb, "Neutral atmospheric delay in interferometric synthetic aperture radar applications: statistical description and mitigation," *Journal of Geophysical Research: Solid Earth*, vol. 108, no. B5, p. 2231, 2003.

[8] R. Snieder and J. Trampert, "Inverse problems in geophysics," in *Wavefield Inversion*, A. Wirgin, Ed., Vienna: Springer Vienna, 1999, pp. 119–190.

[9] L. Iannini and A. Monti Guarnieri, "Atmospheric phase screen in ground-based radar: statistics and compensation," *IEEE Geoscience and Remote Sensing Letters*, vol. 8, no. 3, pp. 537–541, 2011.

[10] L. Noferini, M. Pieraccini, A. Member, D. Mecatti, S. Member, G. Luzi, C. Atzeni, A. Tamburini, and M. Broccolato, "Permanent scatterers analysis for atmospheric correction in ground-based sar interferometry," vol. 43, no. 7, pp. 1459–1471, 2005.

[11] G. Luzi, M. Pieraccini, D. Mecatti, L. Noferini, G. Guidi, F. Moia, and C. Atzeni, "Ground-based radar interferometry for landslides monitoring: atmospheric and instrumental decorrelation sources on experimental data," *IEEE Transactions on Geoscience and Remote Sensing*, vol. 42, no. 11, pp. 2454–2466, 2004.

[12] R. Iglesias, A. Aguasca, X. Fabregas, J. J. Mallorqui, D. Monells, C. Lopez-Martinez, and L. Pipia, "Ground-based polarimetric sar interferometry for the monitoring of terrain displacement phenomena-part i: theoretical description," *IEEE Journal of Selected Topics in Applied Earth Observations and Remote Sensing*, vol. 8, no. 3, pp. 1–1, 2014.

[13] M. G. Genton, "Separable approximations of space-time covariance matrices," *Environmetrics*, vol. 18, no. 7, pp. 681–695, 2007.

[14] G. I. Taylor, "The spectrum of turbulence," *Proceedings of the Royal Society of London. Series A, Mathematical and Physical Sciences*, pp. 476–490, 1938.

[15] R. S. Bivand, E. J. Pebesma, and V. Gómez-Rubio, "Applied spatial data analysis with r," in *Use R*, vol. 1, 2013, p. 378. arXiv: `0402594v3 [arXiv:cond-mat]`.

[16] S. Baffelli, O. Frey, C. Werner, and I. Hajnsek, "System characterization and polarimetric calibration of the ku-band advanced polarimetric interferometer," in *Proceedings of EUSAR 2016: 11th European Conference on Synthetic Aperture Radar*, 2016.

[17] C. Werner, A. Wiesmann, T. Strozzi, A. Kos, R. Caduff, and U. Wegmüller, "The gpri multi-mode differential interferometric radar for ground-based observations," in *Proceedings of the European Conference on Synthetic Aperture Radar*, VDE, 2012, pp. 304–307.

[18] U. Wegmüller, O. Frey, and C. L. Werner, "Point density reduction in persistent scatterer interferometry," in *European Conference on Synthetic Aperture Radar*, 2012, pp. 673–676.